Design and Fabrication of a Symmetrical Cantilever-Beam Capacitive MEMS Accelerometer for Geophone

Chen Sun[a,b,*], Lian-zhong Yu[a]

[a]Institute of Geology and Geophysics Chinese Academy of Sciences(IGGCAS), No. 19, Beitucheng Western Road, Chaoyang District, 100029, Beijing, P.R.China;
[b]University of Chinese Academy of Sciences, 100049, Beijing, China)
*Corresponding auther, Tel: (+86) 01082998609/15210641647, Fax: N/A,E-mail: sunchen@mail.iggcas.ac.cn;

***Abstract* — A novel symmetrical cantilever-beam sandwich capacitive MEMS accelerometer is designed for the application of geophone. The accelerometer features double-sided beam-mass structure with symmetry, shock protection structure, die vacuum package, large capacitance and high resolution. The chip takes up 6.3mm□5.6mm□2.2mm，while the seismic mass weights about 21mg. Test results has shown that the scale factor of the mechanical device reaches 10pF/g, the Q value is 58 and the resonant frequency is 825Hz. The device was connected with closed-loop interface circuit and calibrated, and its second-order nonlinearity is smaller than 0.2%, the cross-sensitivity reaches 0.07% and noise floor is -119dBg/rt(Hz) @200Hz. This type of design has potential advantage of being vacuum packaged at wafer-level.**

Key words*：*Sandwich capacitive accelerometer; Package-level vacuum; 4-layer silicon fusion bonding; Low-noise

I. INTRODUCTION

In recent years we see growing demand in deep/ultra-deep geological structure oil/gas exploitation which increases drilling cost in orders of magnitude. In order to reduce the risk of drilling, seismic-reflection surveys must provide higher resolution images for those difficult geological structure targets. To achieve this, tens of thousands or millions of geophones with high sensitivity and broad bandwidth are needed to get dense sampling for the seismic reflective wave-field.

Conventional geophone typically uses a spring-mounted magnetic mass moving within a metal coil. It converts velocity of the ground motion into analog voltage signal according to the Faraday's law of induction. This kind of geophone limits the capability of seismic-reflection surveys because: 1) Dynamic range is less than 60dB so it cannot simultaneously acquire strong and weak signals, 2) Low sensitivity and narrow bandwidth make it impossible to acquire high resolution low and high frequency signals from deep geological structures at the same time, 3) Cross-sensitivity is higher than 40% so it can't distinguish P-wave from S-wave, 4) Sensitive to electromagnetic interference.

MEMS digital geophone has great improvement in performance[1,2] over conventional one. It converts acceleration of the ground motion directly into digital signals. Comparing with conventional geophone, MEMS digital geophone has many advantages: 1) Dynamic range reaches 120dB, 2) Bandwidth ranges from 0 to 500Hz, 3) Cross-sensitivity is lower than 1%, which can be used in 3D seismic exploitation to distinguish P and S waves, 4) insensitive to electromagnetic interference. Besides, MEMS digital geophone with low power consumption and miniature size combined with mass production for itself and IC chip certainly can meet the geophone requirements for high density data collection, reliability and lower cost.

MEMS accelerometer is comprised of mechanical device and readout circuit. According to different types of the mechanical device MEMS accelerometer can be divided into comb-drive type and parallel plate sandwich type. The critical dimension of both types are the gap of the capacitors. For the comb-drive type the gap dimension is defined by precision of lithography so the process flow is simple. Meanwhile, mechanical damping of comb-drive structure is inherently lower under given pressure compared with parallel plate sandwich type. However, comb-drive type generally has smaller capacitance and proof-mass due to the device layer thickness and gap width limitation by DRIE(Deep Reactive Ion Etch) aspect ratio[3] . Therefore, high vacuum packaging is necessary to reach high sensitivity. For the sandwich type, the gap dimension is defined by bonding gap of two wafers so the process flow is complex and damping is higher under given pressure. However, the proof-mass is bigger since whole thickness of one or two wafers can be used to form the proof-mass and area of the capacitor is big to reach high sensitivity.

In recent years MEMS digital geophone products are supplied by Sercel Co.[4] and WesternGeco Co.[5] . In 2013, Sercel Co. introduced 508XT seismic data acquisition system using comb-drive type MEMS accelerometer. In 2012, WesternGeco Co. introduced

multi-measurement towed-marine seismic system using sandwich type MEMS accelerometer. Besides, sandwich type accelerometer produced by Colibrys Co.[6] meet the requirement of seismic survey. Also a sandwich type accelerometer with vacuum package[7] and with symmetrical structure using SOI wafer[8] or double SOI wafer[9] were reported.

This paper designed and fabricated a sandwich type accelerometer using symmetrical two cantilever beams and couple of tiny beams as protection structure. Four wafers were fusion bonded to form proof-mass and cover plate. Due to silicon material creep at high temperature fusion bonding our cantilever-beam design eliminates such effect and keeps the performance of the accelerometer stable and consistent.

II. DESIGN

Mechanical device of the accelerometer comprises a proof-mass and two fixed plates. The proof-mass is suspended by cantilever beams with one end fixed at the surrounded frame as shown in Fig.1. Cantilever beams A are more suitable for the high temperature fusion bonding and tiny beams B are used to share stress during shocking. Proof mass C is fabricated by two bonded EPI-silicon wafer.

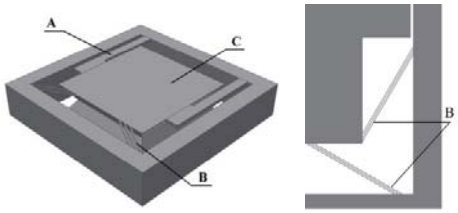

Fig.1 Proof-mass and frame of mechanical device

The top and bottom cover plate will be bonded to the center mass wafer frame to establish two differential capacitors structure. External acceleration causes the proof-mass to move accordingly and changes two capacitors in opposite direction. The differential result of these two capacitors will be measured by the read out circuit and converted into voltage signal as indicated below:

$$\Delta C = \frac{\varepsilon S}{d-\Delta z} - \frac{\varepsilon S}{d+\Delta z} = \frac{2\varepsilon S}{d^2-\Delta z^2}\Delta z \tag{1}$$

$$\Delta V = \frac{\Delta C}{C_{Ref}} V_{Ref} \tag{2}$$

where *S* is the area, *d* is the gap of the capacitor. To increase the signal noise ratio(SNR), differential output should be as large as possible, which requires the large capacitance area and small gap. However, due to device size limitation and gap size control by fabrication process the optimal gap size for our device was chosen as 1.6um to achieve high sensitivity and better yield.

High resolution and broad bandwith are required by the seismic-reflection survey so the accelerometer should reach the noise floor of 400 $\mathrm{ng}/\sqrt{\mathrm{Hz}}$ to satisfy the 120dB dynamic range under 0.4g full range. Meanwhile a consistent full amplitude and phase response of the acceleration signal should cover the frequency range from 1Hz to 500Hz. The major parameters to the design include: 1) M—mass of the proof-mass, 2) ω_0 —resonant frequency, and 3) Q—quality factor.

M is the main parameter to define noise floor of the mechanical device. Low noise floor of the device insures the detection of the weak seismic reflection signal. Noise floor is generally expressed as noise equivalent acceleration[10] :

$$a_{noisefloor} = \sqrt{a_{mea}^2 + a_{eea}^2} \tag{3}$$

Where a_{eea} is equivalent acceleration determined by the read out circuit, and a_{mea} is equivalent acceleration determined by the Brown motion of the mechanical device:

$$a_{mea} = \sqrt{\frac{4k_B T\omega_0}{MQ}} \tag{4}$$

Where k_B is the Boltzmann constant, *T* is the Kelvin temperature. According to (4), either increase M or Q will lower the noise floor. Here we use two bonded wafers for the proof mass fabrication to get maximum available mass for the device. The proof –mass is designed as a quadrate with dimension of 3300um and the mass is about 21mg.

Resonant frequency ω_0 is priorly set. The mechanical device is a typical 2nd order system, whose frequency response is mainly determained by ω_0 and Q as show in Fig.2.

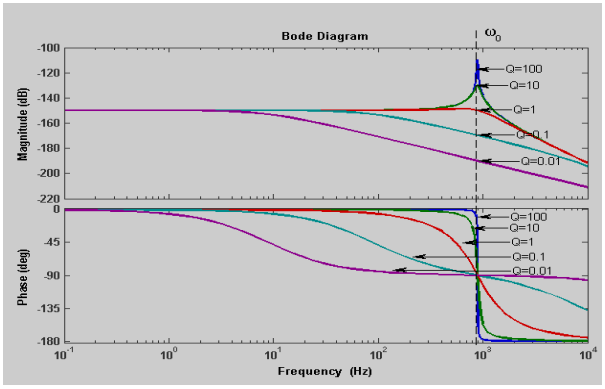

Fig.2 Frequency response of typical 2nd order system

In order to have a flat curve of amplitude and phase response in frequency range from 1Hz to 500Hz we designed the first modal frequency to be 888Hz so $\omega_0 = 2\pi \times 888 = 5579$ rad /s. Then Q is designed to be about 60 to satisfy the system stability as well. The calculation of noise floor for the mechanical device can reach 27$ng/\sqrt{Hz}$.

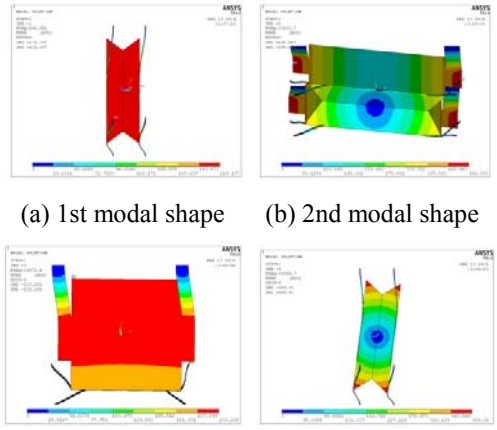

(a) 1st modal shape (b) 2nd modal shape

(c) 3rd modal shape (d) 4th modal shape

Fig.3 First 4 modal shapes

TABLE I.COMPARISON OF MODAL FREQUENCIES

	ω_i(Hz)	ω_i/ω_1
1	888	1
2	10893	12.27
3	19073	21.48
4	30056	33.85

Fig.3 a, b, c, d shows the first to fourth modal shapes. The first modal shape is vibration of proof-mass along sensing axis, and the second modal shape is angular vibration of proof-mass along the axis parallel with beam. The second modal frequency is 12 times that of the first mode, which means the cross sensitivity is suppressed because the second modal frequency is far away from the first one.

Q is determained by the damping caused by gas sealed in the device:

$$Q = \frac{1}{2\zeta} \tag{5}$$

$$\zeta = \frac{c}{2M\omega_0} \tag{6}$$

Where ζ is the damping ratio, c is the damping coefficient [11] ,

$$c = 2 \times \frac{\mu L B^3 \beta(B/L)}{d^3} \tag{7}$$

Where B is the length and L is the width of the plate of the capacitor. $B = L$=3300um, and coefficient $\beta(B/L) \approx 0.42$. μ is the coefficient of viscosity of air under normal temperature and pressure and it's value is about 1.8×10^{-5}Pa·s. d=1.6um is the gap of the capacitor. It could be calculated $\zeta \approx 1867 \gg 1$ so $Q \ll 0.01$, which means under normal temperature and pressure the mechanical device is severely over-damped limiting the noise floor and the bandwith.

To improve Q a vent-hole is designed in the frame to ventilate the device, and vacuum will be achieved in package level by using getter. Besides, grooves with depth over 150um are etched on the plates of cap-wafer to further improve damping effect.

III. FABRICATION

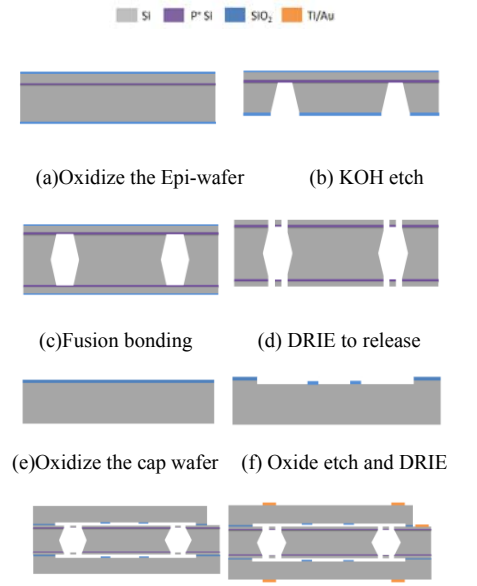

(a)Oxidize the Epi-wafer (b) KOH etch

(c)Fusion bonding (d) DRIE to release

(e)Oxidize the cap wafer (f) Oxide etch and DRIE

(g)3 wafers fusion bonding (h)Sputter Ti/Gold

Fig.4 Process flow

Fig.4 shows the process flow of the fabrication.

①P-type (100) oriented EPI wafer with 20um device layer and 500um handle layer separated by 2um heavily B doped layer was thermal oxidized. (Fig.4(a))

②KOH etch the 500um handle layer using SiO_2 as mask, the heavily B doped layer act as stop layer. (Fig.4(b)).

③Fusion bonding of two etched wafers.(Fig.4(c))

④Release the device by DRIE. (Fig.4(d))

⑤Oxidize double side polished wafer as cap wafer. (Fig.4(e))

⑥Oxide etch. Then the remaining oxide will define the 1.6um gap and bumper that isolate two plates of the capacitor. DRIE will then be used to form damping grooves. (Fig.4(f))

⑦Fusion bond the three wafers at the same time. (Fig.4(g))

⑧Sputter Ti and Gold for wire bonding. (Fig.4(h))

Fig.5 is the optical photo of the cantilever beam and tiny beams. Fig.6 is CT image of the vent-hole of the finalized device. Fig.7 and Fig.8 show damping grooves on the cap and wire bonded device in the package, respectively.

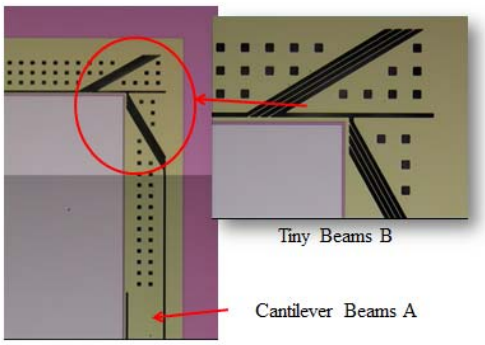

Fig.5 Optical photo of released structure

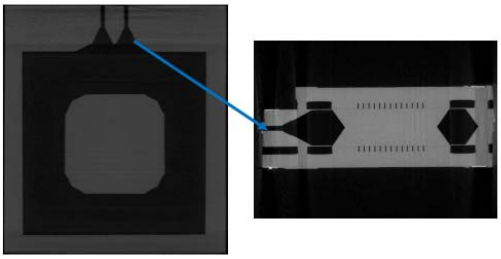

Fig.6 CT image of the vent-hole of the finalized device

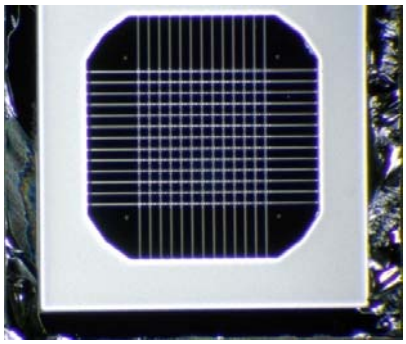

Fig.7 Grooves etched on cap-wafer

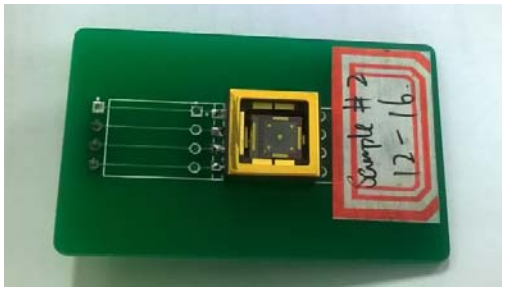

Fig.8 Wire bonded device mounted on PCB board

IV. CHARACTERIZATION

C-V test, Q test, open loop transfer function test and shock test were performed to characterize the mechanical device. Then the device was connected with read out circuit for calibration, after which noise floor was measured.

A. C-V test

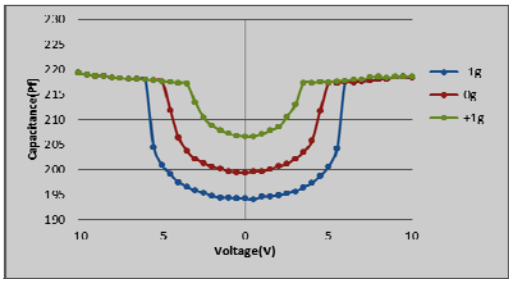

Fig.9 Bottom Capacitor C-V Curve under -1g, 0g, 1g gravity

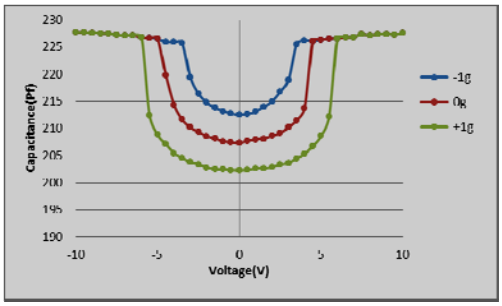

Fig.10 Top Capacitor C-V Curve under -1g, 0g, 1g gravity

Bottom capacitor is referred to the capacitor that is directly mounted to the package and when it faces down the acceleration is 1g for the device.

For each capacitor voltage of DC bias on the capacitor was swept from -10V to 10V. Capacitance change due to different voltage was recorded as shown in Fig.9 and Fig.10. Scale factor of deferential capacitance output of two capacitors is about 10pF/g.

B. Q test

As shown in Fig.11 the unsealed device was placed in a vacuum chamber to simulate package with different pressure. At given pressure a DC bias was given to one capacitor to pull the proof-mass to one side. Then 0V bias

was set to release the proof-mass and its damped oscillation in time domain was recorded to calculate Q value. Typical Time-domain oscillation damping curve is shown in Fig.12.

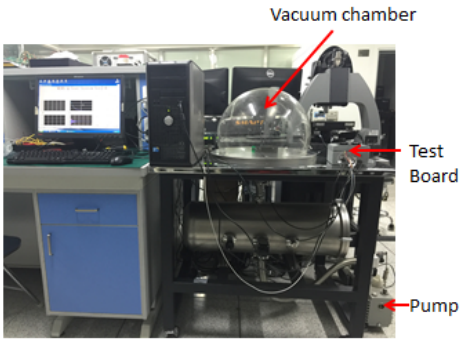

Fig.11 Q-test instrument

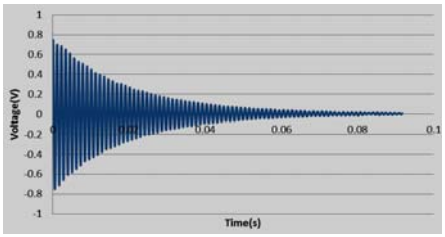

Fig.12 Typical Time-domain oscillation damping curve for Q-value calculation

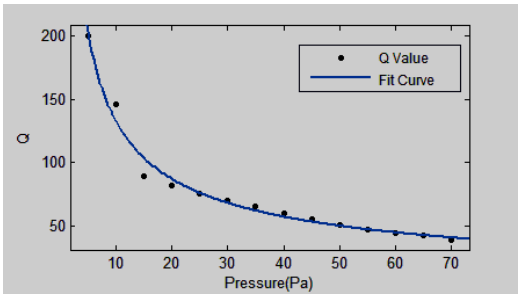

Fig.13 Q vs Pressure

Q value under different pressure is shown in Fig.13. The Q value of vacuum packaged device is 58 so pressure in the package is lower than 45 Pa.

C. Open loop transfer function test

Dynamic signal analyzer Agilent 35670A was used to excite the mechanical device and record its output by time multiplexing method. This test shows the resonant frequency and Q value can be calculated. The test result is shown in Fig.14.

Fig.14 Result of open-loop transfer function

The resonant frequency is 825Hz and Q is 58 which are consistent with the Q test. It can be calculated that the equivalent acceleration determined by the Brown motion of the mechanical device is 27$ng/\sqrt{Hz}$.

D. Shock test

A drop test with 2000g, 0.5ms shock pulse was performed on the device in all 6 directions for total of 60 times. After the shock test the C-V curve of top capacitor under 0g was recorded.

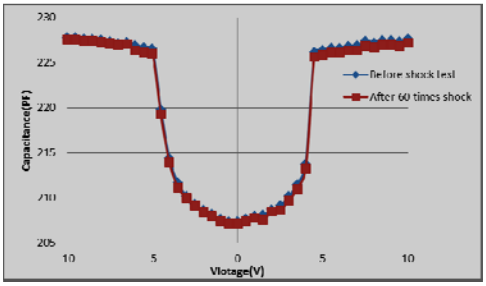

Fig.15 Top Capacitor C-V Curve before and after shock test

As indicated in Fig.15, the C-V curve remains the same which means the device functioned well after the shock.

E. Calibration

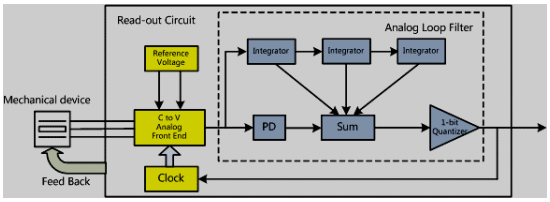

Fig.16 Mechanical device with closed-loop circuit

The mechanical device was connected with the read-out circuit to form a close loop accelerometer as shown in Fig.16. Then the accelerometer was mounted on the rotating motor which placed in temperature controlled chamber to record output under different acceleration for calibration. Mathematical model[12] for calibration is expressed as:

$$A_{ind} = \frac{E_o}{K_1} = K_0 + a_i + K_2 a_i^2 + K_3 a_i^3 + \delta_o a_p - \delta_p a_o + K_{ip} a_i a_p + K_{io} a_i a_o \qquad (8)$$

Where A_{ind} is acceleration indicated by the accelerometer in g. E_o is accelerometer output in g/bit. a_i、a_p、a_o is applied acceleration components along the positive input, pendulous and output references axes, respectively in g. K_0 is bias in g. K_1 is scale factor in bit/g. K_2 is 6econd-order nonlinearity coefficient in g/g^2. K_3 is third-order nonlinearity coefficient in g/g^3. δ_o、δ_p is misalignments of the input axis with respect to the input reference axis about the output reference and pendulous reference axis, respectively in radians. K_{ip}、K_{io} is cross-coupling coefficients in (g/g)/cross g.

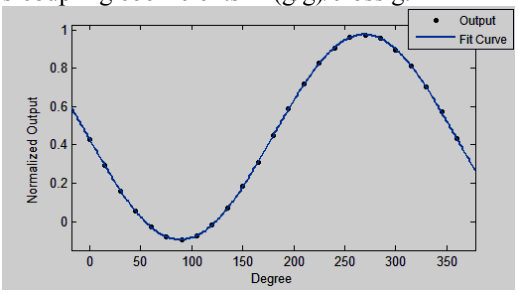

Fig.17 Output under gravity after calibration

Output of accelerometer preliminary calibrated is shown in Fig.17. K_1 is 0.5. K_2 is less than 0.2% and cross-coupling coefficients is less than 0.07%.

E. Noise floor

Noise floor of the vacuum sealed accelerometer was tested.

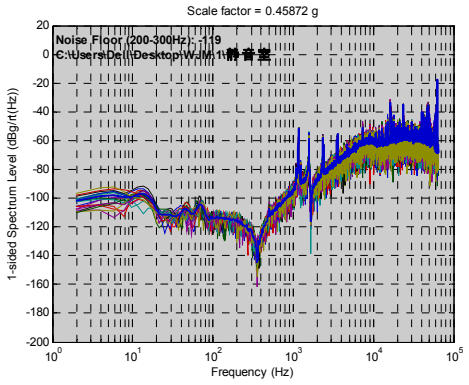

Fig.18 Power spectral density of accelerometer's noise with vacuum sealed device

As indicated in Fig.18 noise floor reached -119dBg/$\sqrt{Hz}$ at 200Hz.

Noise floor will rise if non-vacuum sealed device is used.

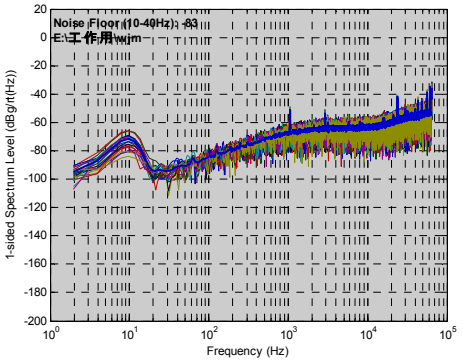

Fig.19 Power spectral density of accelerometer's noise with non-vacuum sealed device

As indicated in Fig.19, the noise floor was about -100dBg/$\sqrt{Hz}$ in 1~200Hz.

V. CONCLUSION

This paper designed and fabricated a novel cantilever-beam sandwich capacitive MEMS accelerometer. Test results showed that the capacitive scale factor is 10pF/g, second-order nonlinearity coefficient is less than 0.2%, cross-coupling coefficient is less than 0.07% and noise floor reached -119dBg/$\sqrt{Hz}$ at 200Hz. The accelerometer features high sensitivity and low cross-sensitivity and can be used to applications which requires high resolution and low cross sensitivity like geophone and inertial navigation. Couple of tiny beams were introduced in the mechanical structure of accelerometer to protect it against external shock. Also this type of design has potential advantage of being vacuum packaged at wafer-level and our next step will be pursuing wafer level package of the die with improved manufacturing process.

ACKNOWLEDGMENT

The authors gratefully acknowledge the support from National S&T Major Project of China under grant (2011ZX05008-005).

REFERENCES

[1] J. Laine and D. Mougenot, Benefits of MEMS based seismic accelerometers for oil exploration, Solid-State Sensors, Actuators and Microsystems Conference, 2007. TRANSDUCERS 2007. International, 1473-1477,2007.

[2] F. Rudolf, A. Jornod, J. Bergqvist and H. Leuthold, Precision accelerometers with μg resolution, Sensors and Actuators A: Physical. 21, pp. 297-302,1990.

[3] B. Wu, A. Kumar and S. Pamarthy, High aspect ratio silicon etch: a review, Journal of Applied Physics. 108, pp. 051101,2010.
[4] J. Laine and D. Mougenot, A high-sensitivity MEMS-based accelerometer, The Leading Edge. 33, pp. 1234-1242,2014.
[5] H. Paulson, V. Husom, N. Goujon and J. Lahdenperä, Introducing Industrial-Grade MEMS Sensors to the Seismic Industry, 2015 SEG Annual Meeting, 249-253,2015.
[6] Colibrys,Data sheet of SF1500S.A-SF1500SN.A / Single axis best in class seismic accelerometer,Datasheet,2007
[7] M.-n. CAI, Y.-l. LIN, L.-f. CHE, R.-t. SU, X.-f. ZHOU and X.-l. LI, Design and fabrication of MEMS acceleration sensor for device-level vacuum packaging, Transducer and Microsystem Technologies. 12, pp. 030,2012.
[8] X. Zhou, L. Che, J. Wu, X. Li and Y. Wang, A novel sandwich capacitive accelerometer with a symmetrical structure fabricated from a D-SOI wafer, Journal of Micromechanics and Microengineering. 22, pp. 085031,2012.
[9] Q. Hu, C. Gao, Y. Hao, Y. Zhang and G. Yang, Low cross-axis sensitivity micro-gravity microelectromechanical system sandwich capacitance accelerometer, Micro & Nano Letters, IET. 6, pp. 510-514,2011.
[10] V. Kaajakari, Practical MEMS: Design of microsystems, accelerometers, gyroscopes, RF MEMS, optical MEMS, and microfluidic systems, Las Vegas, NV: Small Gear Publishing(2009).
[11] M. Bao,Analysis and design principles of MEMS devices,Published by Elsevier,2005.
[12] IEEE,Standard specification format guide and test procedure for linear, single-axis, pendulous, analog torque balance accelerometer,Standard specification,1972